JOURNAL OF MATERIALS SCIENCE 30 (1995) 1313–1320

Effects of manganese dispersoid on the mechanical properties in Al–Zn–Mg alloys

DONG SEOK PARK
Defense Quality Assurance Agency, P.O. Box 276, Cheongryang, Seoul, 130-650, Korea
SOO WOO NAM
Department of Materials Science and Engineering, Korea Advanced Institute of Science and Technology, 373-1, Kusong Dong, Yusung Gu, Taejon, Korea

In order to investigate the strengthening effect of manganese dispersoid in manganese-added Al–Zn–Mg alloys, specially designed alloys with various manganese content were prepared and evaluated. The manganese dispersoid in the alloy is found to increase the strength significantly without losing much elongation. The strengthening effect originates from the fact that the manganese dispersoid behaves as the non-shearable particle which is composed of Al, Mn and Zn. It can be concluded that the improvement of mechanical properties by the manganese dispersoid without losing much elongation is due to the strengthening effect produced by the pinning action of the dispersoid on dislocation glide and the enhancement effect in elongation caused by a homogenization of slip. Meanwhile, the manganese dispersoid and soluble manganese element in the peak-aged manganese-added Al–Zn–Mg alloys are observed not to influence the width of the precipitate-free zones (PFZ) and the kinetics of precipitates such as η' and GP zone (solute rich cluster).

1. Introduction

High-strength aluminium alloys such as Al 7075, Al 7050 and Al 2024 are widely used in many applications for their good combinations of high strength and good resistance to stress corrosion cracking. However, their poor weldability limits their applications. The Al 7039 and Al 7017 aluminium alloys, which have lower strength than Al 7075, are known as promising materials for improving weldability.

It has been reported that the addition of Zr, Cr and Mn in commercial aluminium alloys can form fine dispersoids of 0.03 to 0.3 μm. These dispersoids strongly affect fracture toughness, recrystallization characteristics and grain structure [1–4]. The principal roles of these dispersoids are retardation of recrystallization and grain growth [4–7]. In aluminium alloys zirconium dispersoid, Al_3Zr, is known as the tetragonal and cubic structures that have a unique coherent relationship with the matrix, unlike other dispersoids [7–10], which significantly refines the grain size without raising quench sensitivity [3, 4, 7, 12]. On the other hand, chromium dispersoid, E-phase ($Al_{18}Mg_2Cr_3$), is incoherent with the matrix [9, 10] and increases strength sufficiently while raising quench sensitivity [12]. In the case of manganese dispersoid in an Al–Zn–Mg alloy, even though its crystal structure and composition have not been reported clearly, it has been observed that its size is nearly the same as that of the chromium dispersoid and that it is incoherent with the matrix without raising quench sensitivity [4, 11, 12].

The main purpose of this research is to study the effect of manganese on the tensile properties in Al–Zn–Mg alloys. In addition, the morphology of Mn dispersoid and the effect of Mn dispersoid on the precipitation in Al–Zn–Mg alloys are examined.

2. Experimental procedures

Four kinds of Al–Zn–Mg–Mn alloys were prepared with varying Mn content, as shown in Table I. These alloys were prepared by melting 99.99% pure aluminium, aluminium–manganese master alloy (Mn: 75 wt %) and other alloying elements. For degassing, Ar gas was blown into the melt for 5 min, then poured into a preheated (150 °C) metal mould. The ingots were homogenized by heating for 24 h at 460 °C. The alloys were hot-extruded at 395 °C to make a bar, which was 28 mm thick and 52 mm wide with an extrusion ratio of 11.4. The fabricated alloys were solutionized in air at 460 °C for 90 min followed by quenching in water. These quenched bars were stretched to give about 2.5% strain with a strain rate of $4 \times 10^{-3}\ s^{-1}$, and aged at room temperature for 96 h. To give the maximum yield strength, each alloy was peak-aged by double-ageing [13, 14] at 97 °C for 8 hours and 140 °C for 10 h.

The mechanical properties of the alloys were measured with the standard sub-size sheet type tensile specimen. Its tensile axis was coincident with the longitudinal extruded direction. To observe the effect of manganese on the mechanical behaviour of the alloys,

0022–2461

TABLE I Chemical composition of aluminium alloys (wt %)

Alloy	Zn	Mg	Zr	Mn	Cr	Si	Ti	Al
Alloy 1	4.70	2.80	0.11	0.07	–	0.02	–	balance
Alloy 2	4.38	2.97	0.18	0.50	–	0.01	0.01	balance
Alloy 3	4.11	2.90	0.13	0.68	0.01	–	0.01	balance
Alloy 4	4.20	2.97	0.18	1.13	0.02	0.02	0.01	balance

some of the specimens were solutionized and then tensile tests were carried out.

The microstructures were examined by TEM (Jeol–Jen 200CX) equipped with an energy dispersive X-ray analyser which confirmed the manganese dispersoid. The slip band distribution was examined by TEM with the specimen deformed up to 1% plastic strain. Thin foils were prepared by using the twin-jet polishing technique, using a 70% nitric acid and 30% methanol mixture at $-25\,^{\circ}C$. The image analyser was used to determine the distribution and spacing parameter of the manganese dispersoid. The fracture surface of the tensile specimen was examined using a scanning electron microscope (SEM). To measure the heat of formation of the various precipitates, a differential scanning calorimeter (Perkin Elmer Model DSC4) was used with a scanning rate of $20\,^{\circ}C$/min.

3. Results and discussion

3.1 Microstructure

The typical peak-aged microstructures of the alloys tested in this work are shown in Fig. 1 for the precipitates and precipitate-free zones (PFZ). In order to observe the particles clearly, dark-field images were taken as shown in Fig. 2 in which the marked particles were identified by the analysis of selected area diffraction patterns. Except for the manganese dispersoid resulting from the addition of manganese, all of the alloys were shown to have the same microstructure consisting of η' precipitate and Zr dispersoid (Al_3Zr), regardless of manganese content. However, the GP zone (may be smaller than 10 nm), which is not shown in the dark-field micrograph, is considered to probably coexist with η' precipitate in the matrix of a peak-aged Al–Zn–Mg alloy. Therefore, it is believed that the microstructures of all of the alloys consist of the GP zone, η' precipitate and Zr dispersoid. In addition to these particles, the manganese-containing alloys 2, 3 and 4 are observed to have Mn dispersoid. From this it might be suggested that the addition of manganese to an Al–Zn–Mg alloy does not influence the kinetics of the precipitates such as η' and the GP zone during the two-step ageing treatment.

Fig. 3a, b, c and d show the change in the distribution of the dispersoid with manganese content. These results illustrate that the number of rod-type particles, which are considered to be the manganese dispersoid, increases with the manganese content in each alloy. However, their size and morphology are observed not to be influenced by manganese content. The detailed measurements of the manganese dispersoid are listed in Table II. To analyse the chemical composition of the dispersoid, an X-ray energy dispersive microanalyser in TEM was used, and the result is shown in Fig. 4. In this figure, it is clearly shown that the dispersoid is composed of only Al, Mn and Zn. However, it was impossible to determine the composition quantitatively because we could not get the standard specimen determining the K-constant characterizing the elemental sensitivity and collection efficiency for the elements [15]. We only suppose that these particles are $Al_{24}Mn_5Zn$, since the composition of manganese dispersoid in an Al–Zn–Mg alloy which does not contain other elements such as Fe and Si has been reported to be $Al_{24}Mn_5Zn$ [16].

Consequently, in TEM work it is important to note that the addition of manganese to an Al–Zn–Mg alloy does not influence the kinetics of the conventional precipitation at all, and the density of manganese dispersoid uniquely increases with manganese content without changing its morphology and size.

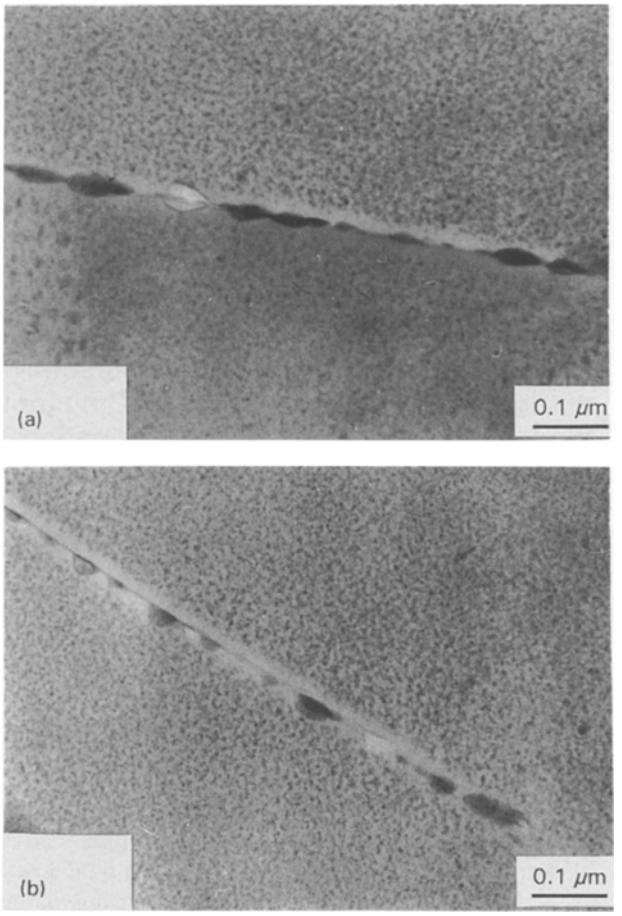

Figure 1 A typical microstructure of matrix without Mn dispersoids showing the same precipitate and PFZ which are independent of manganese content. (a) Alloy 1, (b) Alloy 2.

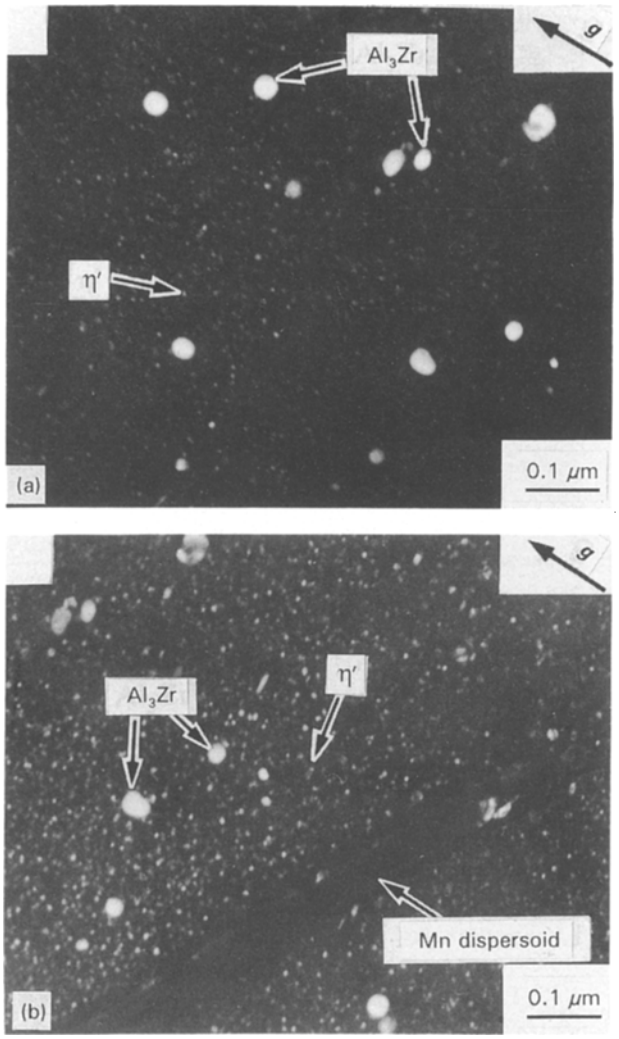

Figure 2 Dark-field transmission electron micrographs showing η′ precipitate, Al_3Z_r particle and Mn dispersoid. B = [0 1 1], g = [0 2 2]. (a) Alloy 1, (b) Alloy 2.

3.2 Differential Scanning Calorimetry (DSC)

To see if the added manganese content influences the kinetics of the precipitates such as GP zone, η′ and η precipitate, differential scanning calorimetry (DSC) was used to measure the heat of formation of the precipitates. The DSC curves for the four alloys, which were peak-aged, are shown in Fig. 5a and b, and the characteristic results from these curves are summarized in Table 3. These results show that the shape of DSC curves and the peak temperature on the first endothermic reaction for each alloy are the same as the characteristics of Al 7050–T6 shown in Alder and Delasis's result [17]. However, the hear of reaction ΔH_R presented in Table III is considerably lower than that found by Alder [17], and this difference is supposed to be caused by the different volume fraction of GP zone and η′ precipitate due to compositional differences such as zinc and magnesium between Al 7050 and our alloys. Thus it is believed that for each alloy the endothermic reaction in the temperature range 160–230 °C corresponds to the dissolution of the GP zone and η′ precipitates in the matrix, since in the DSC technique an endothermic peak describes the dissolution of the existing matrix precipitate, and over the temperature range from near 230 to 280 °C the observed exothermic reactions are considered to be the formation and growth of η′ and η precipitates during DSC analysis. On the other hand, the last endothermic peak in the temperature range 290–390 °C is thought to be associated with the dissolution of η precipitates formed during DSC analysis. From the above DSC results, it can be known that the microstructure of each peak-aged alloy consists of a mixture of GP zone and η′ precipitates as examined in TEM observation.

Meanwhile in the DSC study, the manganese dispersoid in the alloys is not thought to be transformed at all up to the solid solution temperature range, since there is no evidence of the reaction peak up to above 400 °C as shown in Fig. 5a and b. This interpretation seems to be reasonable on the basis of the facts that the manganese or chromium dispersoid was formed from the solid solution during the lengthy homogenizing treatment [18] and casting [19] and that they were not dissolved during solution treatment before ageing [20].

The most important fact is that the DSC results for the four aluminium alloys in the range 0.07–1.13 wt % of Mn, as shown in Fig. 5 and Table III, are very similar to each other, particularly on the peak temperatures and the heat of reaction in the temperature range 160–230 °C. Therefore, elemental manganese and manganese dispersoid in an Al–Zn–Mg alloy could scarcely affect the formation of the precipitates during ageing, and so the role of manganese in the precipitation is entirely different from that of other elements such as Cr and Cu which enhance the formation of η′ or GP zone by increasing the nucleation sites for preferential precipitation [11, 21]. Thomas and Nutting [21] reported that manganese appeared to increase the quantity of GP zone and enhance the growth rate of η′. Bryant [11] also inferred that manganese to a lesser degree could confer upon aluminium alloy an ability to nucleate the preferential precipitation of the solute. However, an increase of η′ precipitation must be due not to Mn but to Cu or preferably Cr, since they used several Al–Zn–Mg alloys containing various amounts of Cu or Cr [22] and did not

TABLE II The characteristics of the manganese dispersoids

Alloy	Particle length (μm)	Particle dia. (μm)	Particle density (m^{-2})	Area fraction	Interspacing (μm)
Alloy 2	0.37 ± 0.15	0.12 ± 0.04	0.52×10^{12}	0.0174	1.15 ± 0.75
Alloy 3	0.30 ± 0.20	0.12 ± 0.04	0.82×10^{12}	0.0464	0.68 ± 0.50
Alloy 4	0.41 ± 0.24	0.15 ± 0.05	1.05×10^{12}	0.12	0.40 ± 0.4

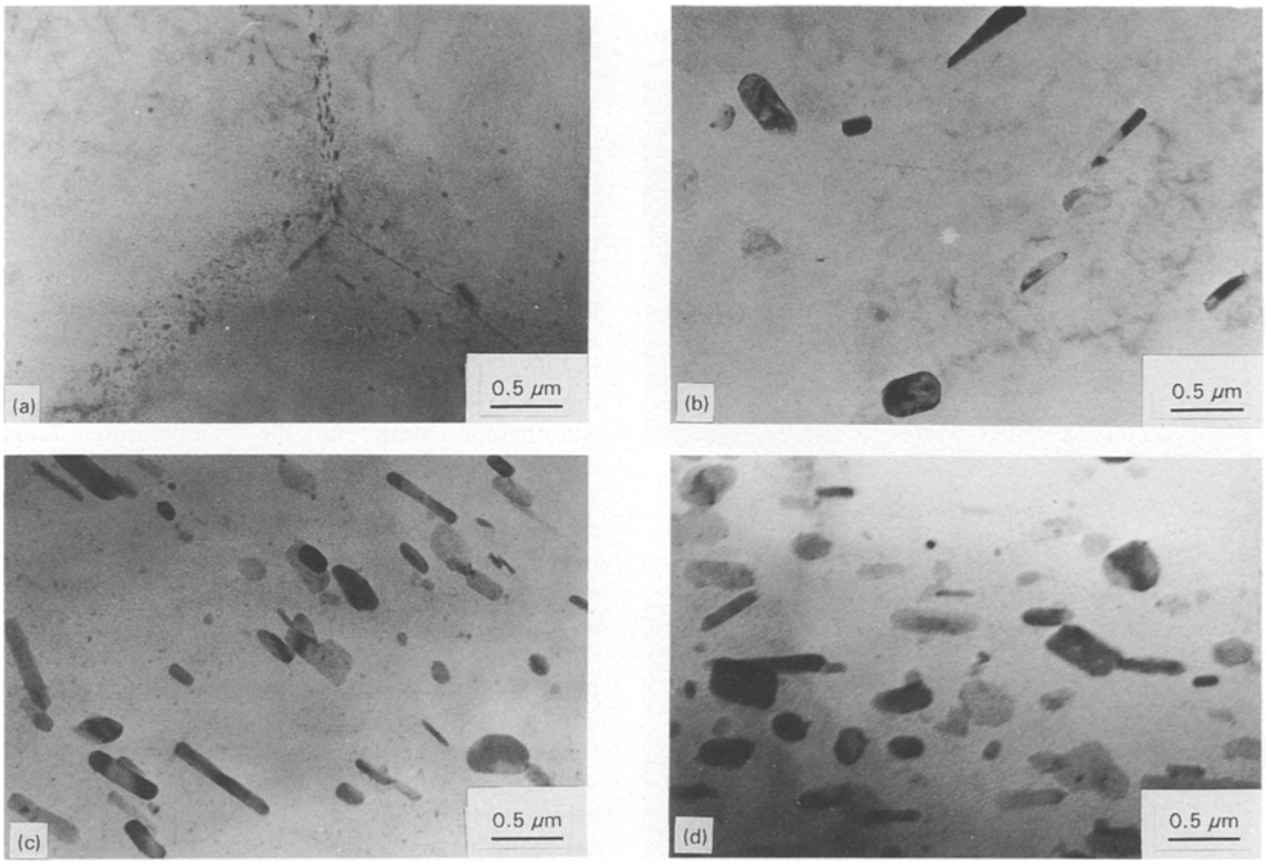

Figure 3 Bright-field transmission electron micrographs showing the effect of Mn content on the distribution of dispersoid. (a) Alloy 1, (b) Alloy 2, (c) Alloy 3, (d) Alloy 4.

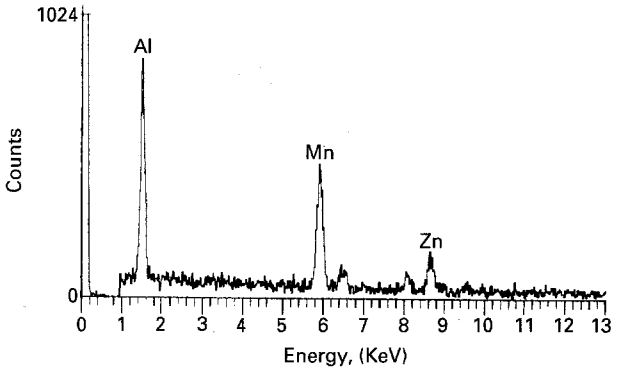

Figure 4 EDS X-ray spectra taken from the Mn dispersoid shown in Fig. 3c.

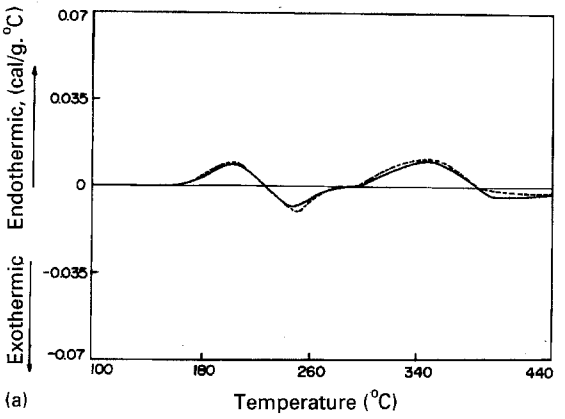

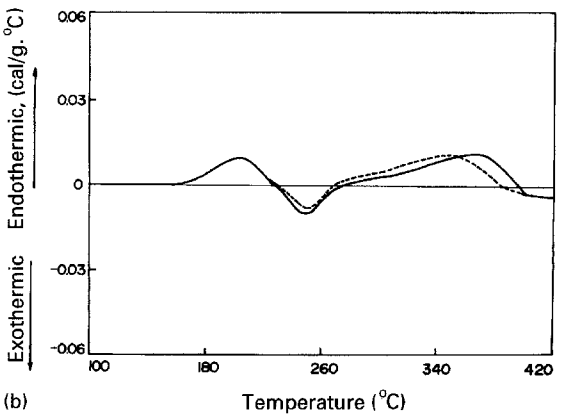

Figure 5 DSC curves of each alloy demonstrating the same characteristics: (a) (– – –) Alloy 1 and (——) Alloy 3, (b) (– – –) Alloy 2 and (——) Alloy 4.

eliminate the possible influence of these extra alloying elements; thus these suggestions cannot easily be accepted. From the above discussion it can be suggested that the manganese dispersoids and soluble elemental manganese in an Al–Zn–Mg alloy not only do not have any effect on the precipitation reaction but also do not provide the nucleation sites for precipitates.

3.3 Mechanical properties

The mechanical properties such as yield strength, ultimate tensile strength (UTS) and elongation for the four alloys are shown in Fig. 6. This shows that the yield strength and ultimate tensile strength

TABLE III DSC characteristics of the Al–Zn–Mg–Mn alloys

Alloy	Region (temp. range, °C)	Peak temp. (°C)	Heat of reaction ΔH_R(Cal/g)
Alloy 1	1 (160–231)	202	1.09 ± 0.1
	2 (231–275)	254	0.61 ± 0.1
Alloy 2	1 (161–234)	202	1.15 ± 0.2
	2 (229–278)	254	0.59 ± 0.1
Alloy 3	1 (167–234)	204	1.12 ± 0.15
	2 (234–287)	253	0.64 ± 0.1
Alloy 4	1 (157–229)	202	1.12 ± 0.15
	2 (229–276)	253	0.71 ± 0.1

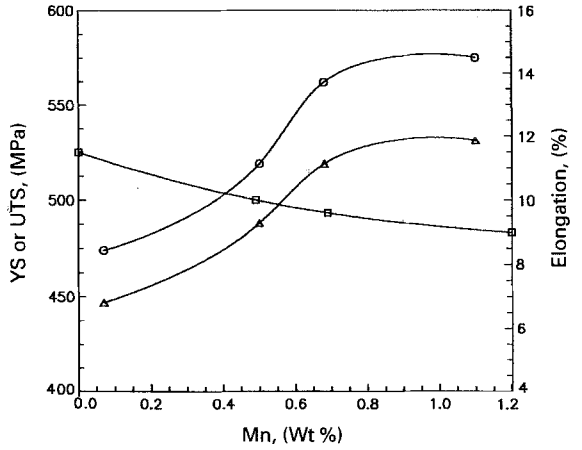

Figure 6 Effect of Mn content on tensile properties ○ UTS, △ YS, □ EL.

significantly increase with the addition of manganese, although there is a slight decrease in elongation. The important finding is that the enhancement of the yield strength and ultimate tensile strength caused by the addition of 0.68 wt % and 1.13 wt % manganese is so significant that the yield and ultimate tensile strength of our alloys are measured to be about 20% higher than those of the best weldable aluminium alloy, Al 7039–T6 [23]. And it should be noted that the UTS of our alloys (Alloys 3 and 4) is even slightly higher than that of the non-weldable Al 7075–T6 [24], which is known to have the highest strength of about 570 MPa (UTS) among 7xxx series alloys.

Regarding the surprising increase in strength, it is believed that the increase in yield strength and ultimate tensile strength without losing much elongation could be caused mainly by manganese dispersoid, since the matrix of the four alloys prepared in this study consists of a very similar mixture of the GP zone and η′ precipitate except for manganese dispersoid. Stoltz and Pelloux [25] reported that chromium and manganese dispersoids are classified as non-shearable particles. Therefore, in our alloys the beneficial improvement in strength from the addition of manganese could be mainly attributed to the manganese dispersoid as the non-shearable particle. In Fig. 3, it can be seen that the density of the manganese dispersoid increases with manganese content. The effects of a manganese content on the size, density, interspacing and area fraction of the dispersoid are presented in Table II. As discussed previously, the size remains almost constant but the interspacing of the dispersoid

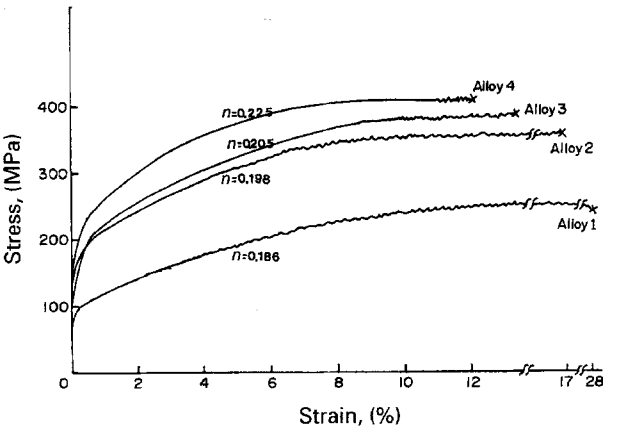

Figure 7 Engineering tensile curves of solution-treated specimens.

drastically decreases with increasing manganese content. Consequently, a dislocation takes higher shear stress to bow around the non-shearable dispersoids, since the shear stress on dislocation bowing by the non-shearable particle is inversely proportional to the particle interspacing.

Fig. 7 can support the discussion mentioned above. It shows that the strength and hardening exponent (n) of the solutionized alloys containing manganese dispersoid only increases with increasing manganese content, but elongation noticeably decreases. Therefore, we can suppose that the non-shearable manganese dispersoid hinders the dislocation motion to enhance the yield strength and ultimate tensile strength as shown in Fig. 6. Furthermore, in Fig. 7, the plastic strain required for the onset of serration for each alloy gradually increases with manganese content. This phenomenon indicates that a solution hardening by Mg contributes considerably to the strengthening of the solutionized specimen of Alloy 1 which contains no manganese dispersoid. On the other hand, a dispersion hardening effect caused by the non-shearable manganese dispersoid may contribute to the strengthening of Alloys 2, 3 and 4 which contain increasing amounts of manganese dispersoid. However, unfortunately it is considered that an Orowan contribution to the yield stress by manganese dispersoid could hardly be evaluated theoretically with the Orowan equation, since there is another effect of manganese, such as grain refinement (See Fig. 9), which can also contribute to the enhancement of the strength of the alloys.

The values of the hardening exponent, n, and uniform elongation, ε_u, defined to be the total strain up to necking, are plotted in Fig. 8, which shows that the values of n and ε_u for the alloys containing manganese are nearly independent of the manganese dispersoid, except for Alloy 1 which contains practically no manganese dispersoid. This result may be explained by the interaction between dislocation and the manganese dispersoid.

Assuming that the manganese dispersoids, as the non-shearable particles, only contribute to work hardening, the UTS will increase and the uniform elongation will significantly decrease due to the reduction of the dislocation mean free path. This fact could almost be recognized by considering that a material containing a dispersion of an intermetallic compound [26]

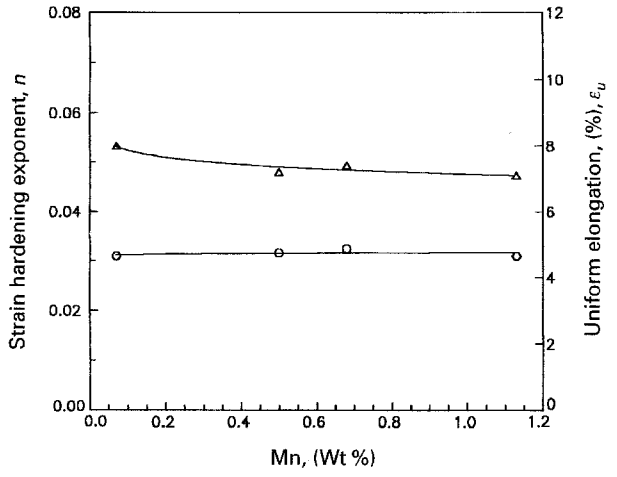

Figure 8 Effect of Mn content on the strain hardening exponent and uniform elongation △ : ε_u; ○ : n.

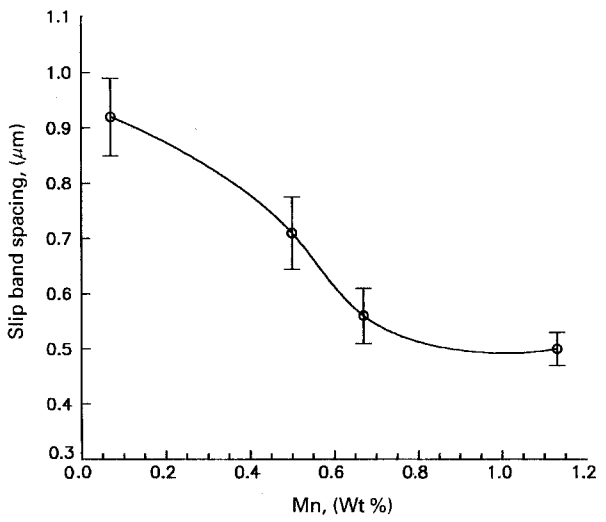

Figure 10 Effect of Mn content on slip spacing.

and a precipitate-hardened aluminium–4.5 wt % copper alloy over-aged [27] could work harden more rapidly than a material without dispersion particles and under-aged aluminium–4.5 wt % copper alloy. If the tensile properties of the manganese-bearing aluminium alloys used in this study also behave in accordance with the above consideration, the UTS and hardening exponent will be increased, and at the same time the uniform elongation will be decreased. However, the results, as indicated in Figs 6 and 8, do not agree with this assumption. Therefore, the phenomenon, which has almost constant values for the hardening exponent and uniform elongation, as shown in Fig. 8, cannot be interpreted according to the above assumption, but may be explained by considering the slip band distribution shown in Fig. 9. In this figure, it can be seen that slip bands are regularly distributed in each grain, each with its own common slip direction, and the width or spacing of the bands is apparently decreased with increasing manganese content to give a homogeneous band distribution. Therefore, a progressive homogenization of slip with increasing density of manganese dispersoid seems to reduce the local strain or stress concentrations, and thus increase the uniform elongation and reduce the hardening exponent. Other workers [28–31] have also reported that

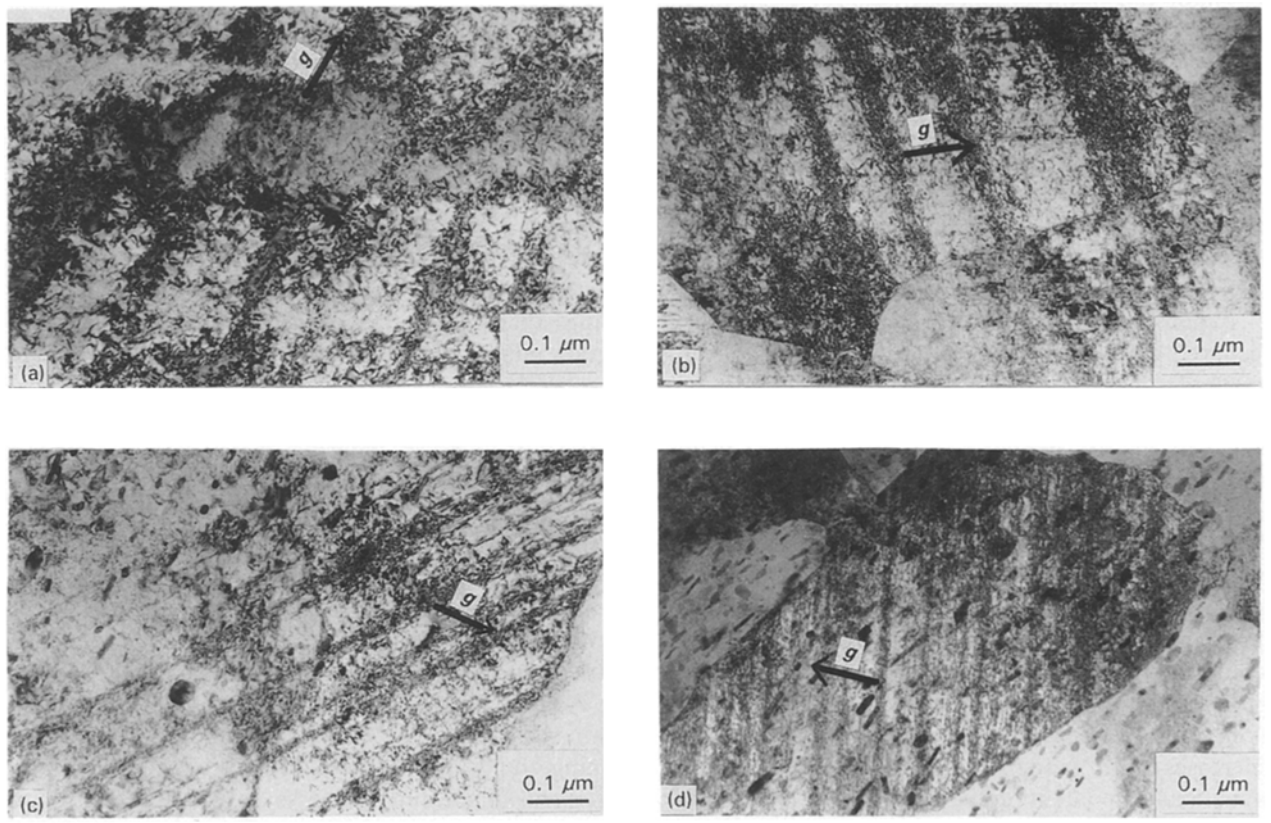

Figure 9 Comparison of the distribution of slip bands after 1% tensile strain: (a) Alloy 1, B = [0 1 3], g = [2 0 0], (b) Alloy 2, B = [0 1 1], g = [0 2 $\bar{2}$], (c) Alloy 3, B = [0 1 1], g = [0 2 $\bar{2}$], (d) Alloy 4, B = [$\bar{1}$ 1 2], g = [2 2 0].

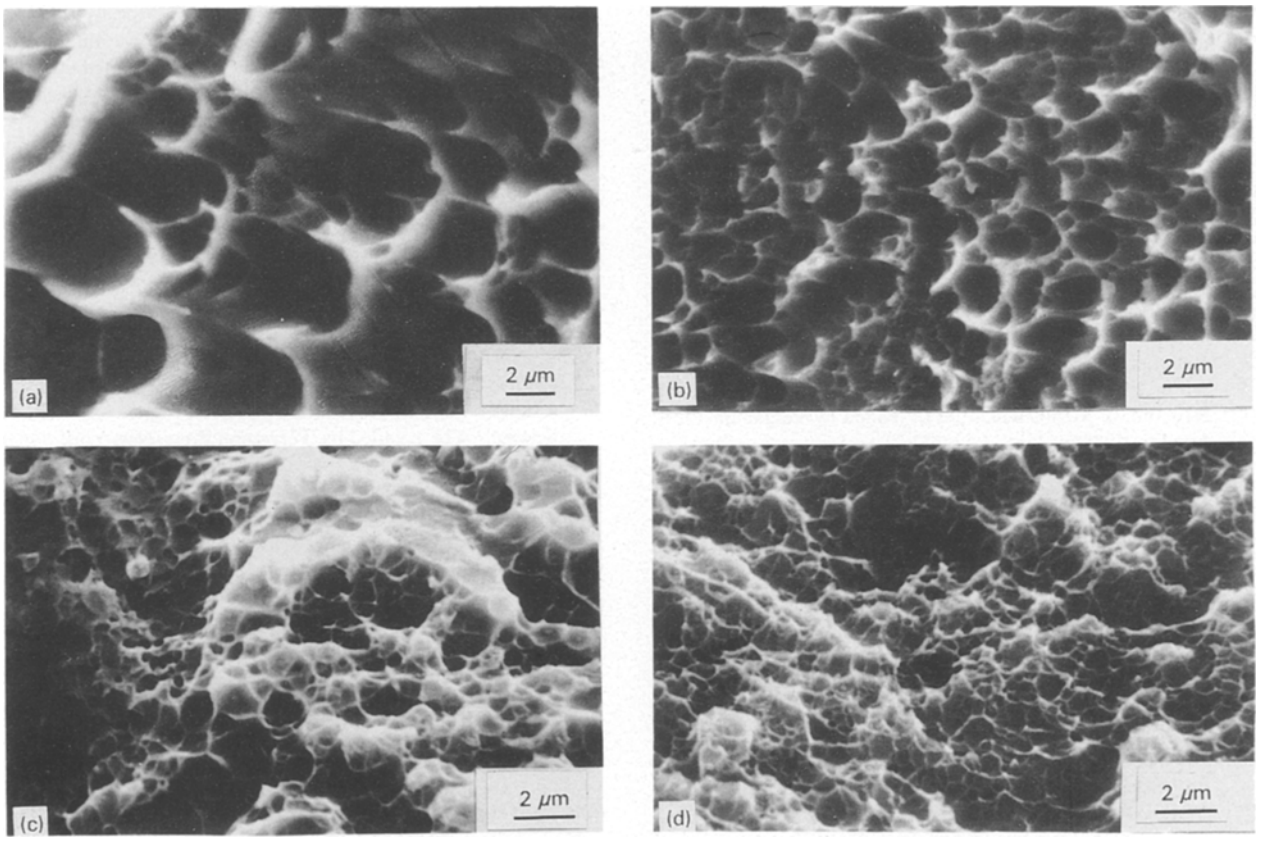

Figure 11 SEM micrographs of the tensile fractured specimens: (a) Alloy 1, (b) Alloy 2, (c) Alloy 3, (d) Alloy 4.

a homogeneous slip occurred in dispersoid-bearing aluminium alloys to enhance the elongation or ductility. In particular, Prince and Martin [29] have suggested that a local strain concentration is proportional to the slip band spacing and grain size (equal to slip band length), and that the maximum slip band spacing produced the maximum strain concentration. In this study the slip band spacing was also observed to decrease with increasing manganese content, as shown in Fig. 10. Moreover, our interpretation mentioned above is suggested on the basis of the observation that the fracture mode, as shown in Fig. 11, is almost the same in each alloy. In Fig. 11, it can be readily seen that the fracture mode is mainly transgranular regardless of the amount of manganese dispersoid, although manganese dispersoid reduces the dimple size noticeably.

From the above discussion about the role of manganese dispersoids in the strengthening effect and a homogenization of slip, we can readily understand that there is an interesting mutual competition between work hardening inducing the increase of the hardening exponent and a homogenization of slip inducing the enhancement of uniform elongation by the manganese dispersoid. Therefore, it can be concluded that the manganese dispersoid makes the slip homogeneous to reduce the local strain or stress concentration, and thus maintains nearly constant uniform elongation and hardening exponent with significant increase in strength.

4. Conclusions

1. The size and morphology of the manganese dispersoid which result from the addition of Mn in an Al–Mg–Zn alloy are independent of manganese content, but its density increases with manganese content. In addition, the manganese dispersoid in an Al–Zn–Mg alloy does not influence the formation GP zone and η' precipitate. Therefore, the microstructures of GP zone, η' precipitate and PFZ for each alloy are almost unchanged, regardless of the density of the manganese dispersoids.

2. The addition of manganese content in the range 0.68–1.13 wt % enhances the yield strength and ultimate tensile strength to a larger extent without much decrease in elongation, since the fine manganese dispersoid can probably work as the non-shearable particle.

3. The manganese dispersoids significantly homogenize slip bands to maintain the elongation or ductility at a certain level since a homogenization of slip can reduce the local stress or strain concentration during plastic deformation.

Acknowledgement

This work was supported by the Korea Science and Engineering Foundation (KSEF) and Ministry of Science and Technology.

References

1. G. G. GARETT and J. F. KNOTT, *Met. Trans.* **9A** (1978) 1187.
2. J. S. SANTNER, *Met. Trans.* **9A** (1978) 769.
3. H. WESTENGEN, L. AURAN and O. REISO, *Aluminum* **57** (1981) 797.
4. *Idem, ibid* **56** (1980) 768.
5. F. H. DIX, Jr., *Trans. ASM* **42** (1950) 1057.
6. VAN LANKER, in "Metallurgy of Aluminum Alloys," (edited by Wiley, New York, 1967) p. 128.
7. R. F. SANDERS, Jr. and E. A. STAKE, Jr., *Mater. Sci. Eng.* **28** (1977) 53.
8. B. THUNDAL and R. SUNDBERG, *J. Inst. Metals.* **97** (1969) 160.
9. W. B. PEARSON, in "Handbook of Lattice Spacing and Structure of Metals and Alloys," (edited by Pergamon Press, London, 1958) p. 138.
10. D. ADENIS, J. P. MOULIN and A. GUILHAUDIS, *Mem. Sci. Rev. Met.* **66** (1966) 135.
11. A. J. BRYANT, *J. Inst. Metals* **94** (1966) 94.
12. D. S. THOMPSON, B. S. SUBRAMANYA, and S. A. LEVY, *Met. Trans.* **2** (1971) 114.
13. W. F. SMITH and N. J. GRANT, *Met. Trans.* **1** (1970) 979.
14. J. LENDAVI, I. KOVACS, T. UNGAR. J. LAKNER and K. BANIZ *Aluminum* **5** (1980) 453.
15. D. B. WILLIAMS, in "Practical Analytical Electron Microscopy in Materials Science," (edited by Verlag Chemie International Bethlehem, PA, 1984) p. 67.
16. L. F. MONDOLFO, in "Aluminium Alloys; Structure and Properties," edited by (Butterworths, London, 1976) p. 847.
17. P. N. ADLER, R. DELASI, *Met. Trans.* **8A** (1977) 1185.
18. D. S. THOMSON, *Met. Trans.* **6A** (1975) 671.
19. A. K. SACHDEV, *ibid.* **21A** (1990) 165.
20. M. O. SPIEDEL, in "International Conference on Fundamental Aspects of Stress Corrosion Cracking," edited by R. W. Staehle, A. J. Forty and D. Van Rooyen (National Association of Corrosion Engineers, Houston, Texas, 1969) p. 561.
21. G. THOMAS and J. NUTTING, *J. Inst. Metals* **88** (1959–60) 81.
22. DONG SEOK PARK and SOO WOO NAM, *J. Mater. Sci. Letters* **10** (1991) 397.
23. E. DI RUSSO, M. CONSERVA, F. GATTO and H. MARKUS, *Met. Trans.* **4** (1973) 113.
24. ASTM Standards, in "Annual Book of ASTM Standards", Section 2 (ASTM, Philadelphia, 1986) p. 329.
25. R. E. STOLTZ and R. M. PELLOUX, *Met. Trans.* **7A** (1976) 1295.
26. A. KELLY and R. B. NICHOLSON, in Progress in Materials Science, " Vol. 1, edited by (Pergamon Press, New York, 1963) p. 306.
27. G. GREETHAN and R. W. K. HONEYCOMBLE, *J. Inst. Metal* **89** (1960–61) 13.
28. J. M. DOWLING and J. W. MARTIN, *Acta Metall.* **24** (1976) 1147.
29. K. C. PINCE and J. W. MARTIN, *ibid.* **27** (1979) 1408.
30. A. K. BUSBY, L. EDWARDS and J. W. MARTIN, *Mater. Sci. and Tech.* **2** (!986) 363.
31. J. A. WALSH, K. V. JATA and E. A. STARKE, *Acta Metall.* **37** (1989) 2861.

Received 30 September 1993
and accepted 27 July 1994